



Comparison of Reacting DDES and LES CFD Simulation Methodologies for a Dual Inlet Ramjet Engine Combustor

Mehmet Burak SOLMAZ^{1, *}, Sıtkı USLU²

¹ Propulsion Systems Division, TUBITAK SAGE, Mamak, 06484, Ankara, Türkiye

² Department of Mechanical Engineering, TED University, Çankaya, 06420, Ankara, Türkiye

ARTICLE INFO

2025, vol. 45, no.1, pp. 10-21
©2025 TIBTD Online.
doi: 10.47480/isibted.1490666

Research Article

Received: 01 June 2024

Accepted: 18 February 2025

* Corresponding Author

e-mail: burak.solmaz@tubitak.gov.tr

Keywords:

Large eddy simulation
Delayed detached eddy simulation
Steady laminar flamelet
Richardson extrapolation

ORCID Numbers in author order:

0000-0003-3571-177X
0000-0003-4734-2625

ABSTRACT

The design of a dual-inlet dump ramjet combustor is critical to the development of a ramjet propulsion system. Parameters such as pressure drop, pressure fluctuations, and combustion efficiency must be evaluated across different flight regimes. In this study, Large Eddy Simulation (LES) and Delayed Detached Eddy Simulation (DDES) techniques, coupled with the Steady Laminar Flamelet combustion model, are used to model a generic ramjet combustor. Grid convergence was ensured through the Richardson extrapolation method, and the grid quality was evaluated using the M-index. Close agreement between both LES and DDES approaches and experimental data confirms their accuracy in simulating the complex flow behaviour of the combustor. The present research demonstrates that the Steady Laminar Flamelet model is capable of predicting flow structures in a ramjet combustor under reacting conditions. In LES simulations, turbulent kinetic energy prediction in the near-wall region was enhanced, leading to faster mixing and an overestimation of combustion efficiency. DDES predictions achieved even closer agreement with experimental data, highlighting the effectiveness of eddy simulation with near-wall modelling when wall resolution is not feasible. This approach demonstrates improved agreement between DDES predictions and experimental data and highlights its efficiency in reducing the need for excessively refined meshes in studying dump-type low subsonic combustors.

Çift Girişli Ramjet Motor Yanma Odası İçin Reaktif DDES ve LES Benzetim Yöntemlerinin Karşılaştırılması

MAKALE BİLGİSİ

Anahtar Kelimeler:

Büyük Burgaç Benzetimi
Gecikmeli Ayrılmış Burgaç Benzetimi
Kararlı Laminer Alevcikler
Richardson ekstrapolasyonu

ÖZET

Çift girişli bir ramjet motoru yanma odasının tasarımı, ramjet itki sistemi geliştirilmesinde kritik öneme sahiptir. Basınç düşüşü, basınç dalgalanmaları ve yanma verimliliği gibi parametreler, çeşitli uçuş rejimleri için ayrı ayrı değerlendirilmelidir. Bu çalışmada, bir ramjet yanma odasını modellemek için Kararlı Laminer Alevcik yanma modeli ile birlikte Büyük Burgaç Benzetimi (LES) ve Gecikmeli Ayrılmış Burgaç Benzetimi (DDES) teknikleri kullanılmıştır. Ağ yapısı yakınsaması, Richardson ekstrapolasyon yöntemi ile sağlanmış ve ağ kalitesi M-indisi kullanılarak değerlendirilmiştir. LES ve DDES yaklaşımları ile deneysel veriler arasında yakın bir uyum gözlemlenmiş ve yanma odasının karmaşık akış davranışı benzetiminde bu tekniklere başvurulabileceği doğrulanmıştır. Mevcut araştırma, Kararlı Laminer Alevcik modelinin bir ramjet yanma odasındaki akış yapısını tahmin etme yeteneğini göstermektedir. LES benzetimlerinde, duvar yakınındaki bölgede türbülanslı kinetik enerji daha yüksek hesaplanmakta ve daha hızlı karışmaya ve yanma verimliliğinin fazla hesaplanmasına yol açmaktadır. Duvara yakın bölgede DDES hesaplamalarının büyük burgaç benzetimine kıyasla deneysel sonuçlara daha yakın değerler bulduğu gözlemlenmiştir. Ağ yapısında duvar kenarı çözünürlüğü sağlanmadığında modellemenin daha doğru sonuçlar doğurduğu anlaşılmaktadır. Bu çalışma, DDES çözümlerinin deneysel sonuçlar ile arasında iyi bir uyum olduğunu göstermesinin yanı sıra düşük sesaltı hızlara sahip yanma odası benzetimlerinde yüksek yoğunluklu ağ yapısı uygulamak mümkün olmadığında bu yöntemin elverişliliğini de vurgulamaktadır.

NOMENCLATURE

a_s	characteristic flamelet strain rate [s^{-1}]	Y	mass fraction of a specie
C	model constant	Z	mixture fraction
d	distance to wall [m]	γ	ratio of specific heats
D	diffusion rate [m^2/s]	Δ	largest grid space of the computational cell [m]
f	function	ε	eddy dissipation
f_{DDES}	DDES model multiplier	ε_f	error of f
G_d	dissipation term of k equation [kg/ms^3]	η	combustion efficiency
g_{ij}	velocity gradient tensor [s^{-1}]	κ	Karman constant
h_t	total enthalpy [J/kg]	λ	thermal conductivity [W/mK]
k	turbulent kinetic energy [m^2/s^2]	μ	dynamic viscosity [$Pa \cdot s$]
l	integral length scale [m]	ν	kinematic viscosity [m^2/s]
P	Probability Density Function	Π	pressure drop
Pr	Prandtl number	ρ	density [kg/m^3]
Q	Q criterion [s^{-2}]	σ	shear stress [Pa]
r_d	a parameter for DDES model	τ_{ij}	subgrid stress tensor [kg/ms^2]
Sc	Schmidt number	ϕ	a variable
S_{ij}	strain rate tensor [s^{-1}]	φ	equivalence ratio
S_{ij}^d	traceless symmetric part of the square of the velocity gradient tensor [s^{-2}]	χ	scalar dissipation rate [s^{-1}]
V	computational cell volume [m^3]	Ω	vorticity tensor [s^{-1}]
u_i	velocity component [m/s]		

INTRODUCTION

The concept of the integrated rocket ramjet was introduced in the 1960s, sparking decades of research into dump combustor design (Fry 2011; Le Pichon and Laverdant 2016; Timnat 1990). Fig. 1 illustrates the primary components of a dual-inlet dump-type integrated rocket ramjet combustor, comprising the primary reactor, secondary reactor, and mixing regions (Kim and Natan 2015; Roux 2009). Incoming air jets generate four corner vortices, while the dump section induces suction, collectively shaping the reactors. Key factors affecting overall ramjet engine performance include reactor size and efficiency, dump effects, air intake dimensions, intake angle and curvature, flow separators in the intake stream, Reynolds number, and combustor dimensions (Chuang et al. 1989; Kim and Natan 2015; Stowe et al. 2004; Stull et al. 1985). The inherent inability to scale ramjet engine combustion chambers (Blevins and Coleman 1999) poses a challenge when evaluating various geometrical configurations and operating conditions through experimentation. As a result, Computational Fluid Dynamics (CFD) becomes a crucial tool for advancing the development of ramjet propulsion engines.

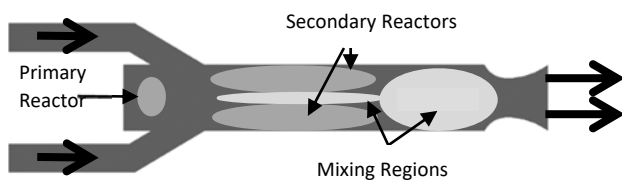


Fig. 1 Reactor zones definition of a dual inlet dump-type ramjet combustor.

A well-defined combustor configuration for understanding the internal dynamics of dual-inlet ramjets is the square cross-section ramjet engine introduced in 1995 by Ristori et al. (1999) and Gicquel et al. (2002). Optically accessible combustor walls made diagnostics possible for Laser Doppler Velocimetry, Particle Image Velocimetry, Planar Laser-Induced Fluorescence and Chemiluminescence. Researchers have used the data from these measurements to enhance the validity of

their CFD predictions (Gicquel et al. 2006; Le Pichon and Laverdant 2016; Reichstadt et al. 2007; Roux et al. 2010).

While addressing the limitations of Reynolds-Averaged Navier-Stokes (RANS) approaches in predicting time-dependent changes within the combustor, an alternative method known as the Unsteady-RANS approach has gained recognition for simulating reactive flows (Nemati, Ong, and Walther 2022; Solmaz, Uslu, and Uzol 2014). However, the Unsteady-RANS computations have constraints in capturing fluctuating components and their associated frequencies, which are crucial performance parameters for ramjet engines (Stull et al. 1985).

In response to these limitations, Large Eddy Simulation (LES) studies have been conducted (Reichstadt et al. 2007) using grids composed of up to 3.4 million hexahedral elements (Roux et al. 2009). While the near-wall flow structures were not resolved with these grids having y^+ values of approximately around 50 but the general flow field was properly predicted.

Researchers have employed various strategies to enhance the quality of LES results, including the application of different combustion models. Additionally, specific modifications were made to one of the global reaction mechanisms, and a more CPU-intensive Eddy Dissipation Concept combustion closure was employed to achieve successful solutions (Roux 2009).

Simulating eddy structures is crucial for accurately assessing the thermoacoustic instability performance of the combustor, a key parameter for ramjet engines. While consistent results have been achieved by researchers (Roux et al. 2010) using Large Eddy Simulation (LES), there is a limitation in simulating near-wall structures due to high y^+ values, which extend beyond the viscous sublayer range. Therefore, a more reliable approach might involve modelling these near-wall structures. The Detached Eddy Simulation (DES), initially proposed by Spalart et al. (1997), offers a hybrid RANS/LES approach that effectively models turbulent structures near the walls, especially those that are computationally expensive to simulate. This method has been further enhanced by

Spalart et al. (2006) with the introduction of a delaying mechanism, which aims to postpone the transition from RANS to LES in scenarios with thick boundary layers.

Numerous successful combustor simulations have been reported in the literature, with several studies demonstrating the capabilities of the DES model such as the work of Sun et al. (2008). However, only a limited number of works, such as Ashoke et al. (2015), have specifically addressed the simulation of dump combustors, a relevant scenario for integrated rocket ramjet technology. In this study, we aim to showcase the potential of the hybrid RANS/LES model for side dump combustors, where low subsonic corner vortices generated after jet-on-jet impingement which play a significant role in the combustion process.

For the present simulations, the Steady Laminar Flamelet (SLF) combustion model is employed which encapsulates the outcomes of detailed chemistry schemes in a tabulated format, thereby accounting for finite-rate chemistry effects. One well-known drawback of this model is its inability to capture slow reactions. In order to see the predictability of the SLF, the results are compared with the predictions of the Flamelet Generated Manifold (FGM) combustion model which has proven its suitability in the case of slow reaction combustion problems (Yang et al., 2020; Cagdas, 2021). The comparison shows that similar results are observed for the given high-temperature air inlet condition with a global equivalence ratio close to stoichiometry. Similar results are obtained as the test case features a high-temperature air inlet with a global equivalence ratio near stoichiometry (Solmaz and Uslu, 2023).

NUMERICAL TOOLS

In this study, we conducted CFD simulations employing two distinct approaches. Firstly, Large Eddy Simulation (LES) was utilized in conjunction with Wall Adapting Local Eddy Viscosity (WALE) subgrid-scale (SGS) modelling. Then Detached Eddy Simulation (DES) is employed with Realizable k - ϵ turbulence model. For the present computations, the commercially available solver ANSYS Fluent R21 was used.

Favre-averaged filtered governing equations, detailed from Eq. (1) to Eq. (3), were employed (Garnier, Adams, and Sagaut 2009). Notably, when comparing the effects of various terms in the equations, the subgrid-scale pressure dilatation term, subgrid-scale viscous dissipation term, and other non-linear terms were found to have minimal impact compared to the convective and diffusive terms (Martín, Piomelli, and Candler 2000). Furthermore, Eq. (4) provides the resolved shear stress, while Eq. (5) to Eq. (9) outline the modelling of subgrid stresses.

$$\frac{\partial \bar{p}}{\partial t} + \frac{\partial \bar{\rho} \tilde{u}_i}{\partial x_i} = 0 \quad (1)$$

$$\frac{\partial \bar{\rho} \tilde{u}_i}{\partial t} + \frac{\partial \bar{\rho} \tilde{u}_i \tilde{u}_j}{\partial x_j} + \frac{\partial \bar{p}}{\partial x_i} - \frac{\partial \bar{\sigma}_{ij}}{\partial x_j} = - \frac{\partial \tau_{ij}}{\partial x_j} \quad (2)$$

$$\frac{\partial \bar{\rho} \tilde{h}_t}{\partial t} + \frac{\partial \bar{\rho} \tilde{u}_i \tilde{h}_t}{\partial x_i} - \frac{\partial \bar{p}}{\partial t} - \tilde{u}_i \frac{\partial \bar{p}}{\partial x_i} - \frac{\partial}{\partial x_i} \left(\lambda \frac{\partial \bar{T}}{\partial x_i} \right) = - \left[\frac{\partial \bar{\rho} (\tilde{u}_i \tilde{h}_t - \tilde{h}_t \tilde{u}_i)}{\partial x_i} \right] \quad (3)$$

$$\bar{\sigma}_{ij} = 2\mu \left(\tilde{S}_{ij} - \frac{1}{3} \delta_{ij} \tilde{S}_{kk} \right) \quad (4)$$

$$\tau_{ij} - \frac{1}{3} \tau_{kk} \delta_{ij} = -2\mu_t \left(\tilde{S}_{ij} - \frac{1}{3} \delta_{ij} \tilde{S}_{kk} \right) \quad (5)$$

$$\tilde{S}_{ij} \equiv \frac{1}{2} \left(\frac{\partial \tilde{u}_i}{\partial x_j} + \frac{\partial \tilde{u}_j}{\partial x_i} \right) \quad (6)$$

$$\mu_t = \rho l_{wale}^2 \frac{(s_{ij}^d s_{ij}^d)^{3/2}}{(s_{ij}^d s_{ij}^d)^{5/2} + (s_{ij}^d s_{ij}^d)^{5/4}} \quad (7)$$

$$l_{wale} = \min \left(\kappa d, C_w V^{1/3} \right) \quad (8)$$

$$S_{ij}^d = \frac{1}{2} (\tilde{g}_{ij}^2 + \tilde{g}_{ji}^2) - \frac{1}{3} \delta_{ij} \tilde{g}_{kk}^2, \quad \tilde{g}_{ij} = \frac{\partial \tilde{u}_i}{\partial x_j} \quad (9)$$

Here, λ , \tilde{h}_t , τ_{ij} , μ_t , δ_{ij} , \tilde{S}_{ij} , l_{wale} , κ , and d stand for thermal conductivity, filtered total enthalpy, subgrid stress tensor, subgrid turbulent viscosity, Kronecker delta, filtered rate of the strain tensor, turbulence length scale, Karman constant and normal distance to the wall respectively. The WALE constant is $C_w = 0.325$. Additionally, a homogenous mesh assumption is adopted for subgrid length calculation. The isotropic part of the subgrid stress tensor is neglected, as the subgrid-scale Mach number effect is negligible for most supersonic flows (Erlebacher et al. 1992). The subgrid enthalpy flux is modelled using a constant turbulent Prandtl number assumption, as given by Eq. (10).

$$\bar{\rho} (\tilde{u}_i \tilde{h}_t - \tilde{u}_i \tilde{h}_t) = - \frac{\mu_t c_p}{Pr_t} \frac{\partial \bar{T}}{\partial x_j} \quad (10)$$

In Eq. (3), it is important to note that there is no source term. Heat generation from reactions is incorporated into the total enthalpy formulation. Total enthalpy is the sum of chemical enthalpy (enthalpy of formation), sensible enthalpy, and kinetic enthalpy. Pre-tabulated chemistry is used for calculations, which is described below. The application of the ideal gas law is justified by the assumption that combustion occurs within the combustion chamber, where the flow remains in the low subsonic range.

The combustor under investigation has two jet inlets, resulting in jet-on-jet impingement that naturally oscillates and creates four circulating vortices in each corner of the combustor. Based on the work of Peters (1984), the steady laminar flamelet model, SLF, was used to account for the finite-rate effects in turbulent reacting flows. It is assumed that a turbulent flame brush consists of flamelets (Williams 1975), which are laminar, one-dimensional having small flame structures. The laminar flame structures are assumed to be dissipated under a certain strain rate which is a function of cross velocity for one-dimensional flame assumption. Figure 2 presents a schematic depiction of a strained laminar flame.

Species transport was modelled using the mixture fraction theory originally developed for diffusion flames (Bilger 1976, Burke and Schumann 1928). Eq. (11) outlines the transport equations for the filtered mean mixture fraction, denoted as \tilde{Z} . Here, μ_{eff} represents turbulent viscosity divided by the turbulent Prandtl number. The variance of the mixture fraction is calculated using the scaling relation method proposed by Pierce and Moin (1998). The definition of the mixture fraction variance is provided in Eq. (12). Mean scalar dissipation is defined based on work of Pierce and Moin (2004) in Eq. (13). In the present simulation, C_{LES} is a scaling constant set to 0.5, Sc_t is turbulent Schmidt number, taken as 0.85, and C_χ is a constant with a value of 2.

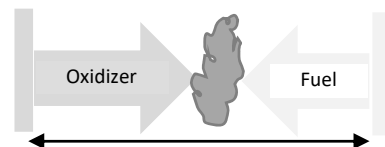


Fig. 2 Strained 1-D flame schematic.

$$\frac{\partial \bar{p}\bar{Z}}{\partial t} + \frac{\partial \bar{p}\bar{u}_i\bar{Z}}{\partial x_i} = \frac{\partial}{\partial x_i} \left(\mu_{eff} \frac{\partial \bar{Z}}{\partial x_i} \right) \quad (11)$$

$$\bar{Z}''^2 = C_{LES} l_{les}^2 \left| \frac{\partial \bar{Z}}{\partial x_i} \right|^2 \quad (12)$$

$$\bar{\chi}_{st} = C_{\chi} \frac{(\mu_t + \mu)}{\rho s c_t} |\nabla \bar{Z}|^2 \quad (13)$$

Species mass fractions are derived from the Steady Laminar Flamelet (SLF) library based on the mean and variance of mixture fraction and scalar dissipation. To prepare for the CFD computations, an opposed-flame chemistry solver is employed to obtain species mass fractions, temperature, density, and enthalpy. These parameters are expressed as functions of mixture fraction, scalar dissipation, and enthalpy. Peters (1984) introduced the transformation of local coordinates to mixture fraction coordinates through the Crocco transformation methodology (Crocco 1940). Further details about this transformation can be found in Peters' original work (1984) or in textbooks such as Poinso and Veynante (2012).

The scalar dissipation rate, denoted as χ , is defined by Eq. (14), where D represents the diffusion coefficient. The scalar dissipation rate at the stoichiometric mixture fraction is referred to as χ_{st} . When applying the laminar flamelet model to the opposed-jet burner, the strain between the flows can be calculated as the velocity difference divided by the distance between the feeding sources. Consequently, the calculation of stoichiometric scalar dissipation can be conducted after solving for the instantaneous mixture fraction within a one-dimensional laminar mixing layer.

Assuming constant density and diffusion coefficient and setting the boundary conditions to 1 and 0 for the fuel and oxidizer zones, respectively, the mixture fraction can be expressed as a function of the diffusion coefficient, strain rate a_s , and location (Peters 1984; Poinso and Veynante 2012). With these boundary conditions for the stoichiometric mixture fraction, the stoichiometric scalar dissipation rate is defined as given in Eq. (15) (Claramunt 2006; Peters 1984; Poinso and Veynante 2012).

$$\chi = 2D \left(\frac{\partial Z}{\partial x_i} \right)^2 \quad (14)$$

$$\chi_{st} = \frac{a_s}{\pi} \exp\{-2[\operatorname{erfc}^{-1}(2Z_{st})]^2\} \quad (15)$$

Where erfc^{-1} is inverse complementary error function. This function is solved using an opposed-flow flame chemistry solver and extinction limits of stoichiometric scalar dissipation rates are calculated. The extension of the equation for variable density and mixture fraction is approximated by Eq. (16) (Claramunt 2006). Here Φ is the variable density effect factor (Kim and Williams, 1997) and is defined by Eq. (17) where ρ_0 represents the density of the oxidiser stream. The combustion pressure is determined from prior CFD calculations, and this value is used to generate tables. Density is corrected for each computation cell using the predefined table pressure, cell pressure, and the ideal gas law during every CFD iteration.

$$\chi = \chi_{st} \frac{\Phi \exp\{-2[\operatorname{erfc}^{-1}(2Z)]^2\}}{\Phi_{st} \exp\{-2[\operatorname{erfc}^{-1}(2Z_{st})]^2\}} \quad (16)$$

$$\Phi = \frac{3}{4} \frac{\left(\sqrt{\frac{\rho_0}{\rho} + 1} \right)^2}{2 \sqrt{\frac{\rho_0}{\rho} + 1}} \quad (17)$$

A look-up table is generated for mixture fraction, its variance, scalar dissipation, and enthalpy. To account for turbulence-chemistry interactions, a Probability Density Function (PDF) is employed. This 4D table includes the compressibility effect by considering enthalpy change. Differences in enthalpy input lead to variations in the output variables of temperature and density. Notably, species mass fraction calculations exclude the effects of enthalpy change due to compressibility, as described by Müller, Breitbach, and Peters in 1994. Species concentrations are assumed to be the same as under adiabatic conditions. The flow chart of the solution methodology is given in Fig. 3.

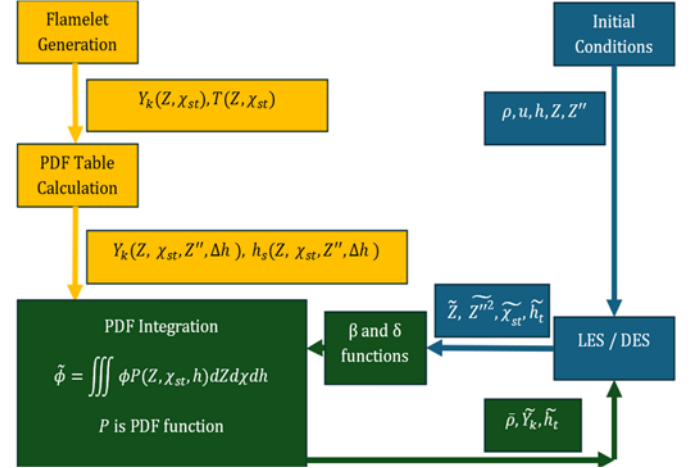


Fig. 3 Solution methodology of numerical framework.

In many applications, resolving near-wall scales is not the primary focus of the problem. Instead of utilizing a subgrid model, Detached Eddy Simulation (DES) employs Reynolds-Averaged Navier-Stokes (RANS) equations within the boundary layer when turbulent length scales become very small, making it impractical to resolve with Large Eddy Simulation (LES). Research conducted by Benim et al. (2008) demonstrated that when the near-wall mesh resolution is insufficient to capture near-wall eddies, DES predictions may yield more accurate results compared to the LES approach.

For problems characterised by thick boundary layers, DES transitions from RANS to LES within the boundary layer. This early switch leads to an incorrect prediction of the viscous sublayer, referred to as Modelled Stress Depletion (Spalart et al. 2006). To address this issue, Delayed DES (DDES) was introduced, specifically designed for situations where the cell edge length is smaller than the boundary layer thickness (Spalart et al. 2006).

In this study, the Realizable k - ϵ model with two equations is utilized for DDES formulation. This model is based on the eddy viscosity similarity concept applied to k -equation models, as proposed by Travin et al. (2002). Turbulent length selection is given in Eq. (18) where C_{DES} is a model constant (0.61), Δ is the largest edge of the computational cell and f_{DDES} serves as the multiplier of the turbulent length scale. The second term on the right-hand side of the equation becomes zero if l_{RANS} is smaller than l_{LES} which is the switch mechanism used by DDES. f_{DDES} and l_{RANS} are defined by Equations (19) to (21).

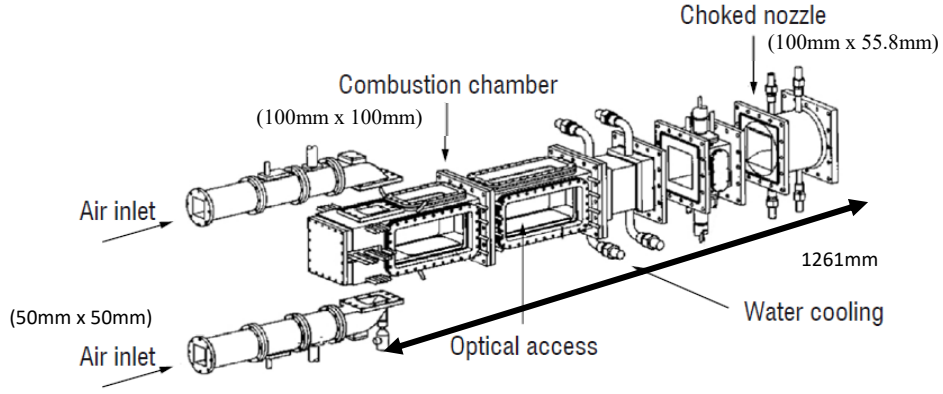


Fig. 4 Sketch of the modular experimental ramjet setup (Le Pichon and Laverdant 2016).

$$l_{DDES} = l_{RANS} - f_{DDES} \max(0, l_{RANS} - C_{DES} \Delta) \quad (18)$$

$$f_{DDES} = 1 - \tanh((20r_d)^3) \quad (19)$$

$$r_d = \frac{v_t + \nu}{\kappa^2 d^2 \sqrt{\frac{\partial u_i \partial u_i}{\partial x_j \partial x_j}}} \quad (20)$$

$$l_{RANS} = \frac{k^{3/2}}{\varepsilon} \quad (21)$$

Here, v_t represents the modelled kinematic viscosity, ν is the molecular kinematic viscosity, and k and ε are calculated using the realizable $k - \varepsilon$ model formulations (Shih et al. 1995). The dissipation term in the k equation, $G_d = \rho\varepsilon$, is reorganized by introducing the DES length scale to connect the kinetic energy production with DES formulation. The new dissipation term is defined by Eq. (22).

$$G_d = \frac{\rho k^{3/2}}{l_{DDES}} \quad (22)$$

Second and fourth-order temperature dependent polynomials are defined for thermal conductivity and viscosity respectively which are calculated by ANSYS Chemkin diffusion opposed-flow flame solver and curve-fitted with MATLAB R2021b. The GRI-Mech 3.0 (Smith et al. 1999) reaction mechanism and its thermal and transport data are used in all chemistry calculations.

EXPERIMENTAL WORK

The results of the experimental work performed by Ristori et al. (1999) were used for the validation of the simulation results. The research ramjet experimental combustor test setup has dual side air intakes with 50 mm x 50 mm cross-section areas connected to the main combustion chamber that has a square in shape of 100 mm x 100 mm as seen in Fig. 4. Electrically heated air is fed into the air inlets through choked nozzles. The combustor is 1261 millimetres long. A choked nozzle with a 55.8 mm x 100 mm throat size is located at the end of the combustor. Gaseous propane fuel is delivered via two tubes from a pre-injection chamber to the combustor. The chamber's metal walls are water-cooled.

Velocity measurements are carried out using Particle Doppler Anemometry, Laser Doppler Velocimetry, and Particle Image Velocimetry, with data collected through quartz-glass side windows. Flame diagnostics are conducted using OH* and CH* Chemiluminescence, as well as Plane Laser-Induced Fluorescence to measure OH and CH emissions (Le Pichon and Laverdant 2016; Roux 2009; Ristori 1999; Gicquel et al. 2002). This study focused on one of the published flight regimes, characterised by an inlet total temperature of 750 K and a mass

flow rate of 0.9 kg/s. The fuel equivalence ratio for the operating condition designated as the "high altitude regime" is 0.75. total temperature of the fuel is 350 K.

COMPUTATIONAL DOMAIN and METHODOLOGY

Multiblock unstructured hexahedral meshing is used throughout the entire computational domain, except for the pre-injection region where polyhedral meshing was utilized. For the discretisation of momentum fluxes, a second-order bounded central differencing discretisation method is implemented.

The hexahedral-polyhedral meshing approach offers the distinct advantage of reducing the total number of grid elements compared to tetrahedral meshing. An axial plane section of the mesh is presented in Fig. 5. The analysis utilised two million cells. To ensure mesh quality, the expansion ratio of the computational mesh was maintained below 1.2, with values primarily around 1.1.

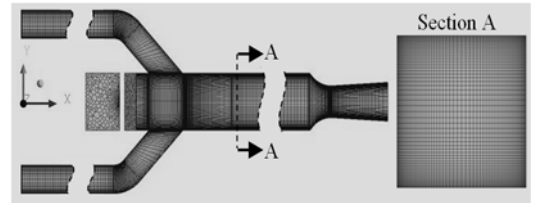


Fig. 5 Cross-section of studied mesh for LES and DDES analysis.

With 20 inner iterations and a bounded second-order implicit differencing scheme, the DDES analyses were initiated using an initial guess derived from an Unsteady RANS result. The results of the DDES analyses were used as the initial state for LES computations. Pressure monitors were strategically placed at various locations to track the convergence of flow dynamics. The cases were run for a minimum of 50 milliseconds before data collection for statistical analysis of the unsteady flow.

Verification Study

To assess the accuracy and spatial convergence of the employed mathematical models, a series of tests were conducted using three sets of meshes containing 0.6, 2.0, and 7.5 million cells, respectively. Only LES simulations were performed for the coarse and fine mesh cases. Combustion efficiency, pressure drop across the engine and the M-index were selected as observables which are defined by Eqs. (23)-(26). The M-index, a theoretical parameter proposed by Pope (2004) as an indicator of mesh quality, was evaluated for LES solutions. M-index is the ratio of modelled subgrid kinetic energy to total kinetic energy (resolved plus modelled).

$$\eta_{comb.eff.} = \frac{T_{t4} - T_{t2}}{T_a - T_{t2}} \quad (23)$$

$$\Pi_{2-4} = 1 - \frac{P_{t2} - P_{t4}}{P_{t2}} \quad (24)$$

$$k_{sgs}(x, t) = \left(\frac{\mu_t}{\rho l_{wale}} \right)^2 \quad (25)$$

$$M_index = \frac{k_{sgs}}{k_{sgs} + k_{resolved}} \leq 0.2 \quad (26)$$

Where T_a is adiabatic flame temperature and it is calculated by ANSYS Chemkin Perfectly Stirred Reactor Solver with a sufficiently long time definition. The subscript t in Eqs. (23) and (24) indicates the total value. The station four in these equations is accepted as the cross-sectional plane close to the start of the converging duct, and the second station of the engine is accepted as inlets. The M-index comparison was performed for volume-averaged values.

For the exact value estimation of any function f , and its error \in following Eqs. (27) and (28) were used (Roy 2010). The cell size is derived from volumetric average of whole domain, and it is found as 4.7 mm, 3.2 mm and 2.3 mm for *coarse*, *medium* and *fine meshes* respectively. Since second-order discretisation schemes were used for transport equations, *order* is taken as 2. The *coarse* to *medium* cell size ratio and the *medium* to *fine* cell size ratio are very similar. Therefore, no modifications were applied to Eq. (27). Decay of error was observed for all parameters given in Fig. 6.

$$f = f_{fine} + \left\{ \frac{(f_{fine} - f_{medium})}{\left(\left(\frac{v_{medium}^{1/3}}{v_{fine}^{1/3}} \right)^{order} - 1 \right)} \right\} \quad (27)$$

$$\in_f = f - f_{mesh} \quad (28)$$

To demonstrate that the mesh employed is sufficiently fine to capture large eddy structures, the M-index value was examined across the entire domain. An acceptable computational mesh for Large Eddy Simulation (LES) calculations is characterised by an M-index value of less than 20%, indicating that 80% of the turbulent kinetic energy is resolved (Pope, 2004). The M-Index, illustrated in Fig. 7 reveals that only approximately 5% of the Turbulent Kinetic Energy within the combustor is modelled.

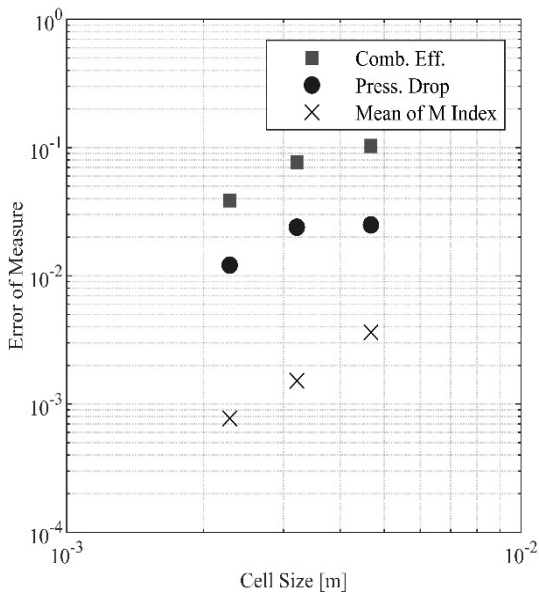


Fig. 6 Error decay due to mesh size in log-log scale of parameters; combustion efficiency, pressure drop and mean of M-index.

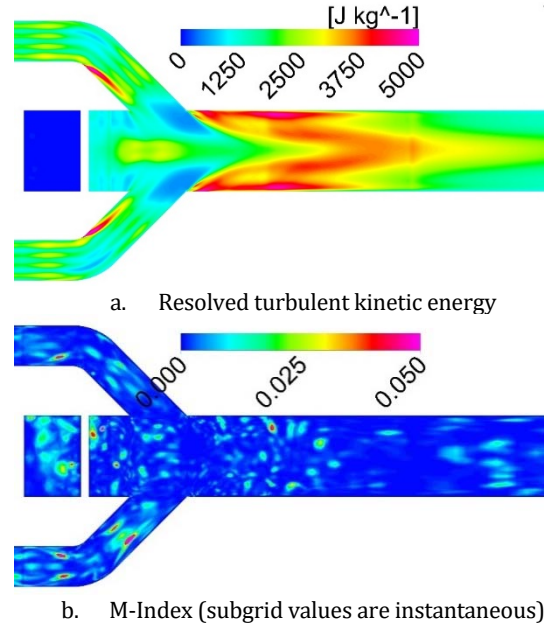
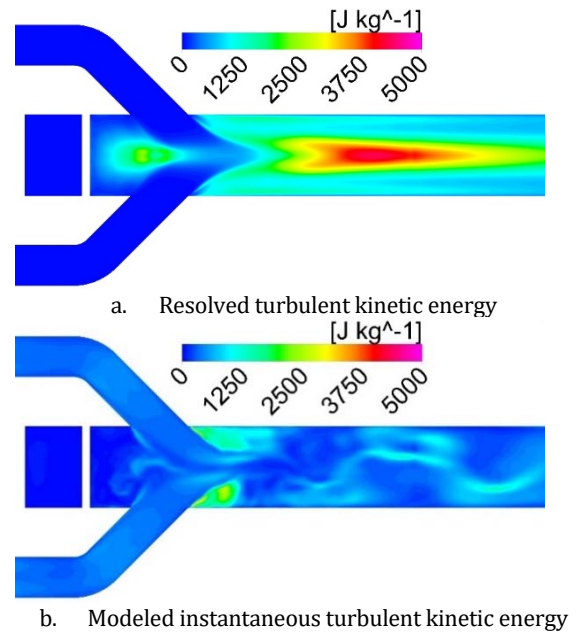


Fig. 7 Resolved turbulent kinetic energy and M-Index distribution (LES).

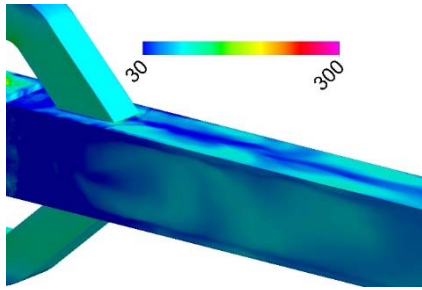
For the Delayed Detached Eddy Simulation (DDES) simulations, the y^+ value, which serves as a reliable indicator of near-wall resolution, assumes significant importance. y^+ values above 30 were predominantly utilized across most of the domain, as depicted in Fig. 8.

Validation Study

This section presents a comparison of the mean normalised axial velocity results for three computational grids along the axial line starting from the combustion chamber's dome, compared with experimental data (Roux et al., 2009), as illustrated in Fig. 9. The simulations demonstrate a strong ability to predict outcomes, particularly in the region after the air inlet jets. Although the difference is not more than 10%, medium and fine meshes have better consistency, which is an indicator of mesh convergence. The findings of verification and validation studies confirm that an acceptable mesh is used for LES and DDES simulations.



b. Modeled instantaneous turbulent kinetic energy



c. Instantaneous y^+ distribution over walls

Fig. 8 Turbulent kinetic energy and y^+ distribution (DDES).

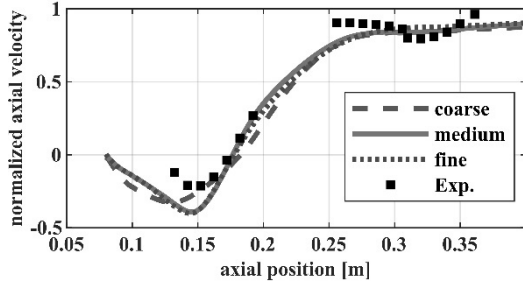


Fig. 9 Mesh study: Normalized axial velocity along the centre line of combustor.

RESULTS

Turbulent kinetic energy contours are displayed in Fig. 7(a) and Fig. 8(a) for LES and DDES computations respectively. When compared to the LES solution, the DDES approach yields lower levels of resolved turbulent kinetic energy, particularly in the air intakes and secondary combustion zones. The prediction of reduced Turbulent Kinetic Energy in the secondary combustion zone is attributed to differences in wall modelling. Lower Turbulent Kinetic Energy leads to a decrease in the mixing rate, thereby delaying the temperature increase. The implications of these results are discussed in this section.

Mean static pressure contours for DDES and LES computations are displayed in Fig. 10. LES computations predict a slightly lower pressure spot near the combustor dome, while the pressure distribution inside the combustor differs only marginally between DDES and LES computations.

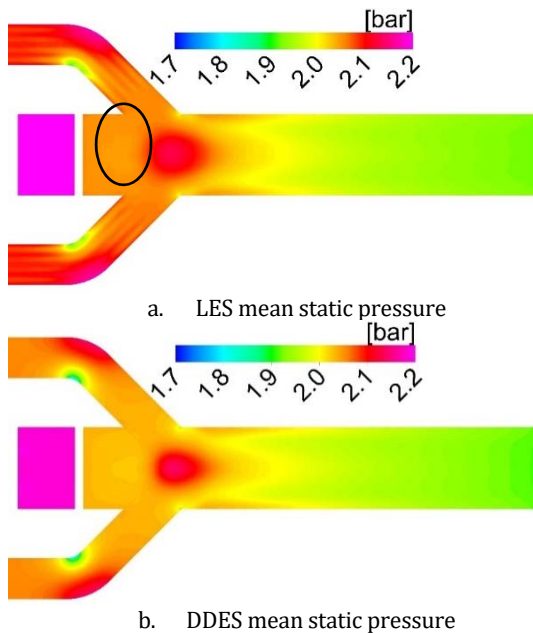


Fig. 10 Time-averaged static pressure contours on mid-plane.

Fig. 11(a) and (b) depict the time-averaged normalized mean axial velocity distribution within the computational domain for LES and DDES computations, respectively. A minor discrepancy is observed in the axial velocity between the two computations. In the case of LES, early flow expansion is noted, attributed to enhanced mixing and consequently higher reaction rates in the early stages of the combustor.

Mean static temperature contours on two planes for LES and DDES are shown in Fig. 12. Both approaches predict a temperature of approximately 1500K in the vicinity of the crossing jets. Due to enhanced fuel-air mixing predicted by the LES approach, it yields a more uniform and higher temperature in each cross-section along the combustor.

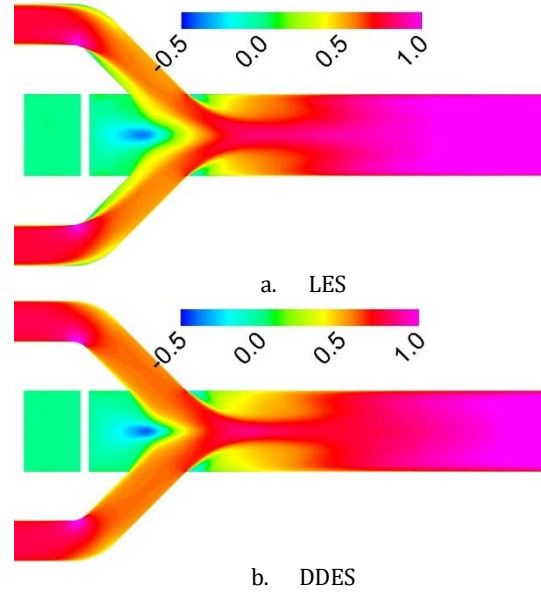
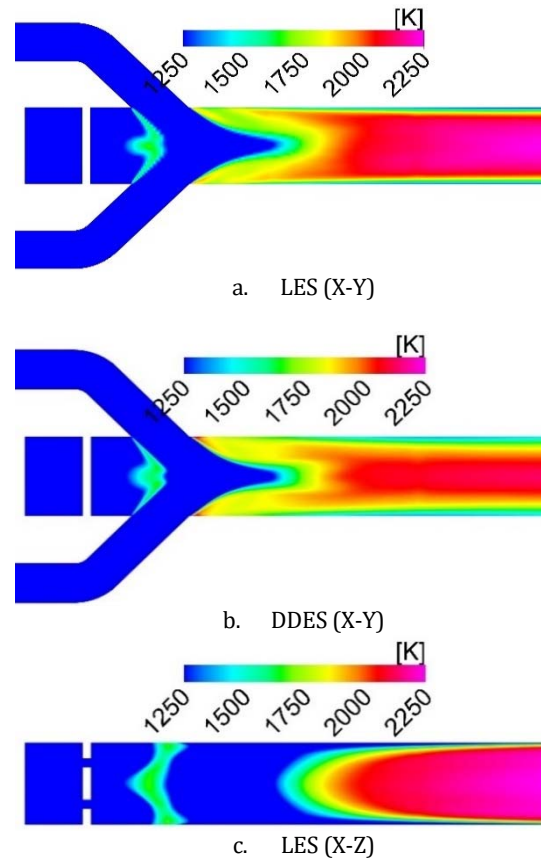
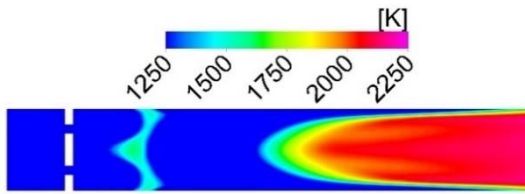


Fig. 11 Time-averaged normalized mean axial velocity contours on mid-plane.





d. DDES (X-Z)

Fig. 12 Time-averaged static temperature contours on mid-plane.

Fig. 13 displays the mass flow-averaged total temperature distribution obtained from planes positioned every 50 mm along the combustor axis. The positions of the planes are indicated in the bottom right corner of the figure. LES computations indicate a temperature 44 K higher at the dump section ($x=200$ mm). A maximum temperature difference of 196 K between the two simulations is observed around the middle of the combustor. The temperature discrepancy diminishes to a value of 28 K at the end of the combustor, corresponding to a 2% lower combustion efficiency. Fig. 14 presents mean equivalence ratio (ϕ) contours calculated from the mean of the mixture fraction. The figure reveals that LES predicts a 50% higher fuel/air ratio at the beginning of the secondary reactor. The higher temperatures computed by LES simulations result in early flow expansion, as seen in Fig. 11.

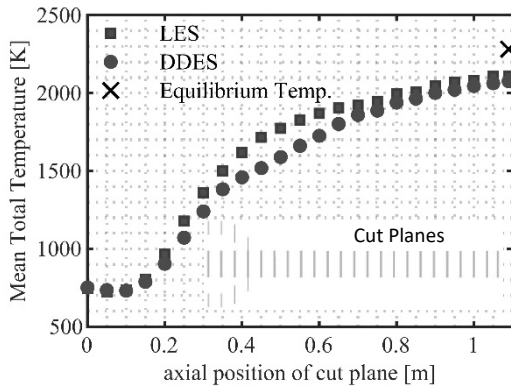
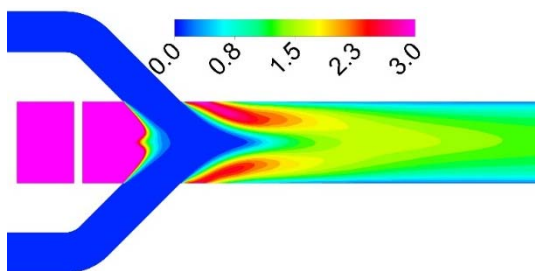
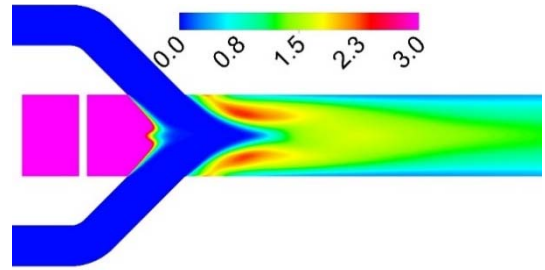


Fig. 13 Mass flow-averaged mean total temperature variation on the planes along the combustor axis.

Instantaneous velocity vectors at $x=200$ mm and $x=300$ mm planes are presented in Fig. 15, with vectors color-coded by OH mass fraction. Four secondary flow vortices are formed in the corners. It's worth noting that the location and shape of these corner vortices calculated at $x=200$ mm exhibit slight differences between the DDES and LES approaches. DDES, by virtue of its use of the RANS formulation, mitigates near-wall eddy generation in the boundary layer. Notably, elevated OH mass fractions are observed at the edges of these vortices. As indicated in the $x=200$ mm vector plot, a hot gas flow emanating from the dome follows these vortices into the secondary reaction zone, effectively acting as a preheater to enhance reactions. This phenomenon is also observed in Fig. 16.



a. LES

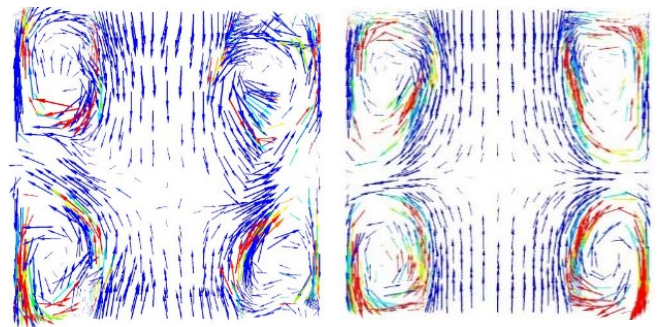


b. DDES

Fig. 14 Mean equivalence ratio contours at mid-plane.

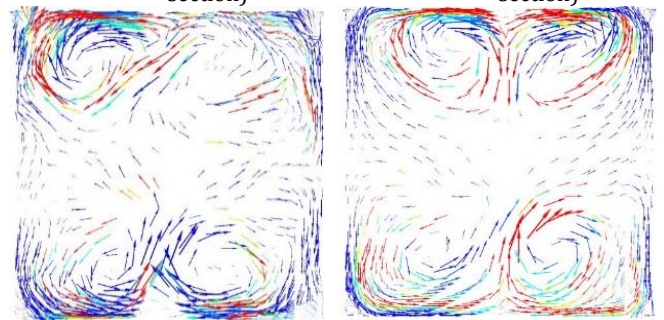
Figure 15 depicts the Q criterion (Hunt, Wray, and Moin 1998), which stands for vorticity tensor. Four main swirling motions (colour-coded by temperature) are generated just downstream of the opposing jets in the combustor. The LES approach predicts a longer main swirling core and numerous small cores around the corners of the combustor. These smaller structures near the corners are induced by near-wall effects. However, it's important to note that the computational cell structure in the boundary layer may not have sufficient resolution for appropriate $x+$ and $z+$ values. Consequently, due to the poor near-wall resolution, small structures on the wall may produce incorrect Turbulent Kinetic Energy. DDES, on the other hand, applies Realizable $k - \epsilon$ formulation in the near-wall region with Boussinesq's hypothesis and is expected to generate more accurate results with boundary cell elements having a high aspect ratio.

Contour plots with a positive Q criterion clearly illustrate the presence of four vortical structures in the corners, as depicted in Fig. 16. This phenomenon underscores the importance of adequately modelling the near-wall region, especially when LES may not effectively resolve it due to non-uniform mesh structures. In this research, the focus is on understanding the success of wall modelling rather than attempting to simulate it using a filter that assumes a uniform cell sizes.



a. LES at 200mm (dump plane section)

b. DDES at 200mm (dump plane section)



c. LES at 300mm

d. DDES at 300mm

Fig. 15 Instantaneous tangential velocity vectors at $x=200$ mm (dump plane) and $x=300$ mm. Coloured by instantaneous OH mass fraction.

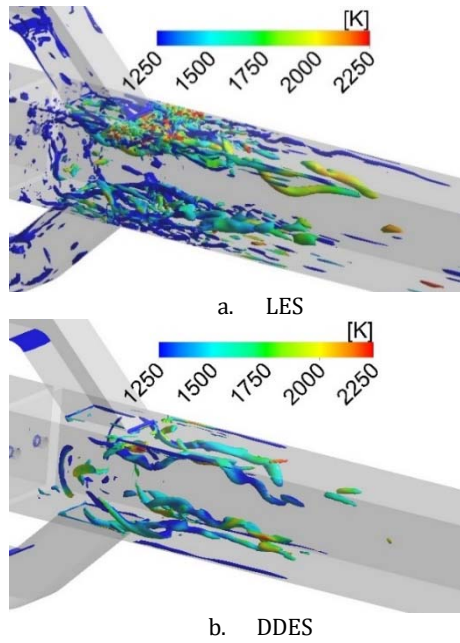


Fig. 16 Q criterion surfaces (positive) coloured with temperature.

The comparison of axial and vertical velocity profiles with measurements along one axial and five vertical lines (as shown in Fig. 17) is presented. Axial velocity profiles along the y-axis are compared with experimental data in Fig. 18. Both the DDES and LES approaches yield very similar results and demonstrate strong agreement with the measured data, particularly in the intersection zone of the jets where the flow field exhibits high complexity due to its inherently three-dimensional structure.

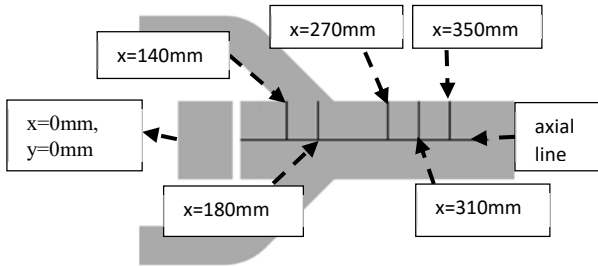


Fig. 17 Experimental measurement lines.

The DDES approach predicted slower flow expansion at the beginning of the secondary zone due to lower temperatures resulting from the previously mentioned slower reactions. This phenomenon is readily visible in the axial velocity profile at $x=270$ mm, where DDES results closely match the measured

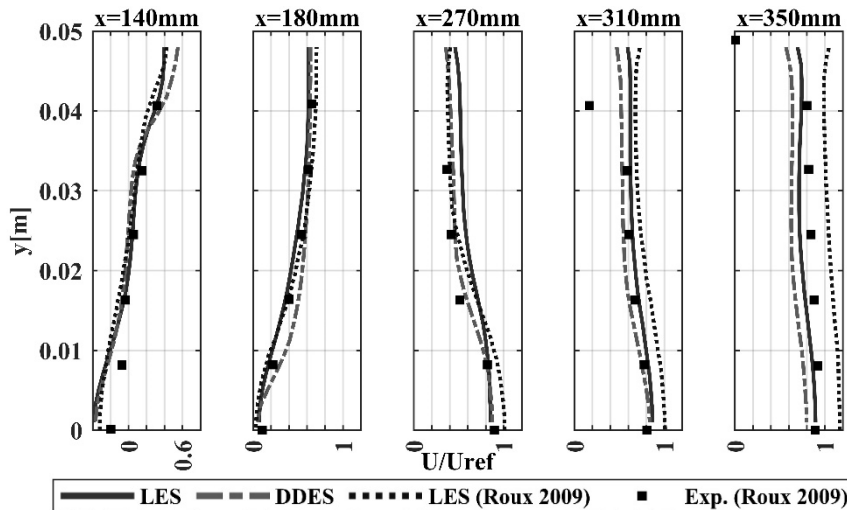


Fig. 18 Normalized axial velocity component along the y-axis (x-axis is the axial velocity normalized by the bulk velocity).

velocity profile. With a more uniform temperature distribution in the vertical direction, the LES approach predicts a smoother velocity profile at $x=350$ mm, aligning well with the measurements. A comparison between the current results and the predictions of Roux et al. (2009) reveals a notably improved agreement with the measured data in the current study, particularly at $x=350$ mm. This improvement can be partly attributed to the utilization of a hexahedral mesh in the current study, as opposed to the tetrahedral mesh used in Roux et al. (2009). However, the primary reason for the discrepancies between the current results and the predictions in Roux et al. (2009) is believed to be related to the combustion modelling approach. Specifically, the Steady Laminar Flamelet (SLF) combustion modelling employed in the current study was compared to the Dynamically Thickened Flame modelling used in the referenced work. Roux et al. (2009) used a single-step chemistry model with five chemical species, resulting in higher adiabatic flame temperatures under rich mixture conditions. These elevated temperatures, as predicted by the Dynamically Thickened Flame model, led to increased flow expansion, with axial velocity being approximately 30% higher than the measurements at $x=350$ mm within the combustor. The axial velocity profiles, particularly at $x=270$ mm, demonstrate a closer agreement when using the Delayed Detached Eddy Simulation (DDES) approach. This can be attributed to the application of a log-law in the near-wall treatment, as opposed to the less conclusive subgrid-scale (SGS) modelling utilized in Large Eddy Simulation.

Fig. 19 presents a comparison of vertical velocity profiles with experimental data. The use of the LES approach results in a more uniform temperature profile within the combustor, leading to greater flow expansion in the axial direction and consequently lower vertical velocity magnitudes. This behaviour agrees well with the experimental data.

Fig. 20 illustrates a comparison of CFD predictions of axial velocity with experimental data along the axis of the combustion chamber. Despite the CFD predictions indicating recirculation that is approximately twice as strong as the experimental data, the velocity field along the axis is well captured. The experimental data exhibit a sharp decrease around $x=310$ mm, marking the end of the secondary reactor zone. Beyond this point, the 3D vortex structures within the secondary reactor zone gradually dissipate, giving way to a strong axial jet. However, CFD simulations fail to predict the steep change in axial velocity observed at $x=310$ mm.

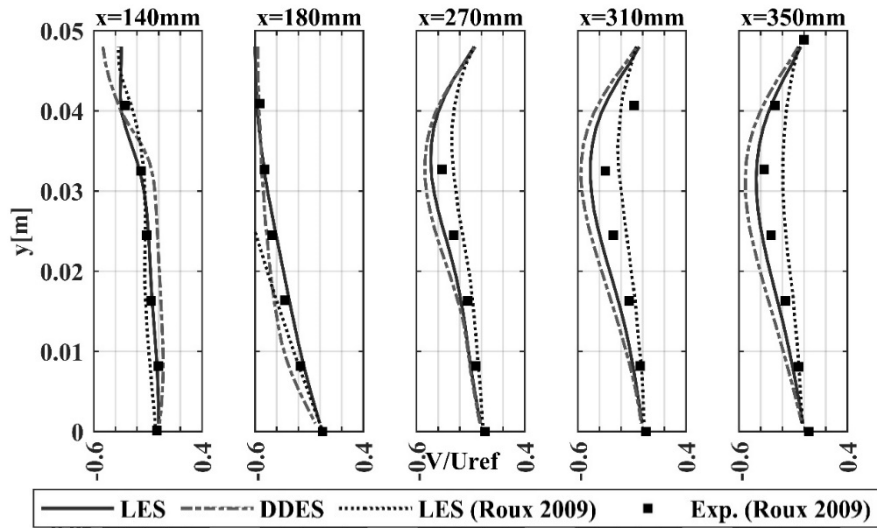


Fig. 19 Normalized vertical velocity component along the y-axis (x-axis is vertical velocity normalized by bulk velocity).

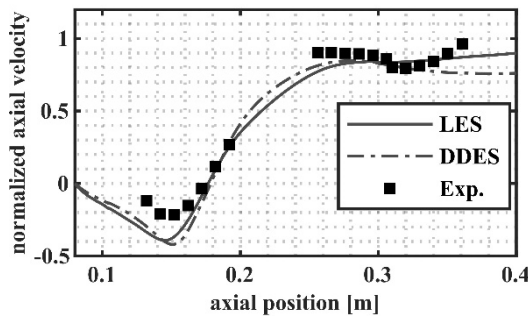


Fig. 20 Axial velocity distribution along the mid-axis.

In terms of integral parameters such as combustion efficiency and pressure drop, there are minor differences between the DDES and LES computations. The LES approach predicts a combustion efficiency of 89%, which is 2% higher than the DDES approach. LES predicts a 5% higher averaged streamline time, which corresponds directly to the combustion "residence time." The near-wall structures in LES enhance mixing, both through residence time and higher turbulent kinetic energy levels, resulting in higher combustion efficiency. Similar findings have been reported in other studies (Le Pichon and Laverdant, 2016) as well. According to Le Pichon and Laverdant (2016), LES predicts a combustion efficiency of 95%, whereas RANS simulations predict an efficiency of 83%. In the same study, however, the measured combustion efficiency was reported as 81%. The authors reported that the reasons for the large disparity between measurements and LES predictions remain unaddressed.

Both approaches accurately predict the pressure drop across the combustor compared to experimental data. The difference between CFD predictions and experimental data lies within the measurement error band reported by Le Pichon and Laverdant (2016). The total pressure loss was measured as 12%, while the simulation result is 11.7%. The total pressure loss is predicted to differ by only 0.5% between DDES and LES computations. The LES prediction of pressure loss is slightly lower.

CONCLUSION

In this study, a wall-modelled LES formulation known as Delayed Detached Eddy Simulation (DDES) is used and the results are compared with those obtained from the LES computations using the Wall-Adapting Local Eddy-Viscosity (WALE) subgrid-scale model in a dual-inlet ramjet combustor.

The findings reveal that both approaches provide good agreement with experimental data on velocity profiles, with only minor discrepancies. However, a noteworthy distinction between DDES and LES lies in the behaviour and distribution of Turbulent Kinetic Energy.

LES with WALE subgrid-scale model tends to predict higher levels of Turbulent Kinetic Energy in the near-wall region compared to DDES, resulting in improved mixing and the formation of an early heated zone. This early combustion phase leads to a greater flow expansion and hence an increase in axial velocity, causing LES with WALE to overestimate axial velocity at $x=270$ mm, whereas DDES predictions align slightly better with the experimental data.

Both DDES and LES simulations overestimate combustion efficiency compared with measurements. However, the total pressure loss is well predicted by both approaches with only a discrepancy of lower than 0.3% compared to measured data that is well within the measurement error range. It's important to note that the overprediction of combustion efficiency remains an open issue, as discussed by other researchers (Le Pichon and Laverdant 2016) also. Future simulations could be extended to calculate heat loss to the walls, which might explain the overprediction of combustion efficiency.

This study demonstrates the promising accuracy of DDES, particularly for simulating a dual-inlet dump-type combustor with a low-subsonic reacting flow field and colliding air jets. DDES, when coupled with the Steady Laminar Flamelet combustion model, exhibited good performance in simulating the flow field and combustion behavior. Although wall-resolving Large Eddy Simulation was not conducted, the results of wall-modelled LES are promising and can serve as a valuable tool for scenarios where a wall-resolving grid is not feasible for industrial applications. Moving forward, our research will focus on using DDES to predict pressure fluctuations, an essential aspect of ramjet combustion. This is identified as a key area for future investigation and improvement.

ACKNOWLEDGMENTS

The authors acknowledge Defence Industries Research and Development Institute of The Scientific and Technological Research Council of Türkiye (TÜBİTAK SAGE) for providing computational resources.

REFERENCES

- Benim, A. C., M. P. Escudier, A. Nahavandi, K. Nickson, and K. J. Syed. 2008. DES Analysis of Confined Turbulent Swirling Flows in the Sub-critical Regime. In *Advances in Hybrid RANS-LES Modelling. Notes on Numerical Fluid Mechanics and Multidisciplinary Design*, ed. S.H. Peng and W. Haase. 97:172-181. Springer-Verlag Berlin Heidelberg. <https://doi.org/10.1007/978-3-540-77815-8>
- Bilger, R. W. 1976. The Structure of Diffusion Flames. *Combustion Science and Technology*. 13:155-70. <https://doi.org/10.1080/00102207608946733>
- Blevins, J. A., and H. W. Coleman. 1999. Apparent Failure of Scaling Methods in Ramjet Connected-Pipe Testing. *Journal of Propulsion and Power*. 15(5):689-98. <https://doi.org/10.2514/2.5480>
- Burke, S. P., and T. E. W. Schumann. 1928. Diffusion Flames. *Industrial & Engineering Chemistry*. 20(10):998-1004. <https://doi.org/10.1021/ie50226a005>
- Cagdas, C.E. 2021. Investigation Of The Relight Characteristics Of A Turbojet Engine Combustion Chamber Under High-Altitude Conditions Using Computational Fluid Dynamics Large Eddy Simulation. M.Sc. Thesis, TOBB University of Economics and Technology Institute of Natural and Applied Sciences Mechanical Engineering Science Programme, Ankara. <http://www.theses.fr/2009INPT025H/document>
- Chuang, C. L., D.L. Cherng, W.H. Hsieh, G.S. Settles, and K.K. Kuo. 1989. Study of Flowfield Structure in a Simulated Solid-Propellant Ducted Rocket Motor. *27th Aerospace Sciences Meeting*. <https://doi.org/10.2514/6.1989-11>
- Claramunt, K., R. Cònsul, D. Carbonell, and C.D. Pérez-Segarra. 2006. Analysis Of The Laminar Flamelet Concept For Nonpremixed Laminar Flames. *Combustion and Flame*. 145(4):845-62. <https://doi.org/10.1016/j.combustflame.2005.11.005>
- Crocco, L. 1940. Sullo strato limite laminare nei gas lungo una parete piana. *Rendiconti del Circolo Matematico di Palermo*. 63:121-75. <https://doi.org/10.1007/BF03015720>
- Erlebacher, G. Y., M. Hussaini, C.G. Speziale, and T.A. Zang. 1992. Toward the large-eddy simulation of compressible turbulent flows. *Journal of Fluid Mechanics*. 238:155-85. <https://doi.org/10.1017/S0022112092001678>
- Fry, R. S. 2011. The U.S. Navy's Contribution to Airbreathing Missile Propulsion Technology. *AIAA Centennial of Naval Aviation Forum "100 Years of Achievement and Progress"*. AIAA Paper 2011-6942. <https://doi.org/10.2514/6.2011-6942>
- Garnier, E., N. Adams, and P. Sagaut. 2009. LES Governing Equations. *Large Eddy Simulation for Compressible Flows*. 1st ed., Springer Netherlands, Dordrecht.
- Gicquel, P., C. Brossard, M. Barat, and A. Ristori. 2002. Experimental Study of a High Speed Flow Inside a Dual Research Ducted Rocket Combustor Using Laser Doppler Velocimetry. *ASME 2002 Fluids Engineering Division Summer Meeting*. ASME Paper FEDSM2002-31432. <https://doi.org/10.1115/FEDSM2002-31432>
- Gicquel, L. Y. M., Y. Sommerer, B. Cuenot, and T. Poinso. 2006. LES and Acoustic Analysis of Turbulent Reacting Flows: Application to a 3D Oscillatory Ramjet Combustor. *44th AIAA Aerospace Sciences Meeting and Exhibit*. AIAA Paper 2006-151. <https://doi.org/10.2514/6.2006-151>
- Hunt, J. C. R., A. A. Wray, and P. Moin. 1988. Eddies, Streams and Convergence Zones in Turbulent Flows. *Proceedings of the Summer Program 1988*. Center for Turbulence Research, Stanford University, Stanford, CA, 1988, pp. 193-208. <https://web.stanford.edu/group/ctr/Summer/201306111537.pdf>
- Kim, S., and B. Natan. 2015. Inlet Geometry and Equivalence Ratio Effects on Combustion in a Ducted Rocket. *Journal of Propulsion and Power*. 31(2):619-31. <https://doi.org/10.2514/1.B35369>
- Kim, J. S., and F. A. Williams. 1997. Extinction of diffusion flames with nonunity Lewis numbers. *Journal of Engineering Mathematics*. 31(2):101-18. <https://doi.org/10.1023/A:1004282110474>
- Le Pichon, T., and A. Laverdant. 2016. Numerical Simulation of Reactive Flows in Ramjet Type Combustors and Associated Validation Experiments. *Journal of Aerospace Lab*. Paper AL11-03. <https://doi.org/10.12762/2016.al11-03>
- Martín, P., M. Piomelli, and G. Candler. 2000. Subgrid-Scale Models for Compressible Large-Eddy Simulations. *Theoretical and Computational Fluid Dynamics*. 13(5):361-76. <https://doi.org/10.1007/PL00020896>
- Müller, C.M., H. Breitbach, and N. Peters. 1994. Partially Premixed Turbulent Flame Propagation in Jet Flames. *Twenty-Fifth Symposium (International) on Combustion*. pp. 1099-1106. [https://doi.org/10.1016/S0082-0784\(06\)80747-2](https://doi.org/10.1016/S0082-0784(06)80747-2)
- Nemati, A., J. Ong, and J. H. Walther. 2022. CFD Analysis of Combustion and Emission Formation Using URANS and LES Under Large Two-Stroke Marine Engine-Like Conditions. *Applied Thermal Engineering*, Vol. 216. <https://doi.org/10.1016/j.applthermaleng.2022.119037>
- Peters, N. 1984. Laminar Diffusion Flamelet Models in Non-Premixed Turbulent Combustion. *Progress in Energy and Combustion Science*. 10(3):319-39. [https://doi.org/10.1016/0360-1285\(84\)90114-X](https://doi.org/10.1016/0360-1285(84)90114-X)
- Pierce, C. D., and P. Moin. 2004. Progress-Variable Approach for Large-Eddy Simulation of Non-Premixed Turbulent Combustion. *Journal of Fluid Mechanics*. 504:73-97. <https://doi.org/10.1017/S0022112004008213>
- Pierce, C. D., and P. Moin. 1998. A Dynamic Model for Subgrid-Scale Variance and Dissipation Rate of a Conserved Scalar. *Physics of Fluids*. 10(12):3041-44. <https://doi.org/10.1063/1.869832>
- Poinso, T., and D. Veynante. 2012. *Theoretical and Numerical Combustion*. 3rd ed., T. Poinso, Toulouse.
- Pope, S. B. 2004. Ten Questions Concerning the Large Eddy Simulation of Turbulent Flows. *New Journal of Physics*. Vol. 6. <https://doi.org/10.1088/1367-2630/6/1/035>

- Reichstadt, S., N. Bertier, A. Ristori, and P. Bruel. 2007. Towards LES of Mixing Processes Inside a Research Ramjet Combustor. *XVIII International Symposium on Air Breathing Engines*. ISABE Paper 2007-1188.
- Ristori, A., G. Heid, A. Cochet, and G. Lavergne. 1999. Experimental and Numerical Study of Turbulent Flow inside a Research SDR Combustor. *35th AIAA/ASME/SAE/ASEE Joint Propulsion Conference and Exhibit*. AIAA Paper 99-2814. <https://doi.org/10.2514/6.1999-2814>
- Roux, A. 2009. Simulation aux Grandes Echelles d'un statoréacteur. Ph.D. Dissertation, Dynamique des Fluides, Institut National Polytechnique de Toulouse. <http://www.theses.fr/2009INPT025H/document>
- Roux, A., S. Reichstadt, N. Bertier, L. Gicquel, F. Vuillot, and T. Poinot. 2009. Comparison of Numerical Methods and Combustion Models for LES of a Ramjet. *Comptes Rendus Mécanique*. 337(6-7):352-361. <https://doi.org/10.1016/j.crme.2009.06.008>
- Roux, A., L. Y. M. Gicquel, S. Reichstadt, N. Bertier, , G. Staffelbach, , F. Vuillot, and T. J. Poinot. 2010. Analysis of Unsteady Reacting Flows and Impact of Chemistry Description in Large Eddy Simulations of Side-Dump Ramjet Combustors. *Combustion and Flame*. 157(1):176-191. <https://doi.org/10.1016/j.combustflame.2009.09.020>
- Roy, C. J., 2010. Review of Discretization Error Estimators in Scientific Computing. *48th AIAA Aerospace Sciences Meeting Including the New Horizons Forum and Aerospace Exposition*. AIAA Paper 2010-126. <https://doi.org/10.2514/6.2010-126>
- Shih, T. H., W.W. Liou, A. Shabbir, Z. Yang, and J. Zhu. 1995. A New k- ϵ Eddy Viscosity Model for High Reynolds Number Turbulent Flows. *Computers & Fluids*. 24(3):227-238. [https://doi.org/10.1016/0045-7930\(94\)00032-T](https://doi.org/10.1016/0045-7930(94)00032-T)
- Smith, G. P., D.M. Golden, M. Frenklach, N.W. Moriarty, B. Eiteneer, M. Goldenberg, C. T. Bowman, R.K. Hanson, S. Song, Jr.W.C. Gardiner, V.V. Lissianski, and Z. Qin. 1999. <http://combustion.berkeley.edu/gri-mech/version30/text30.html>
- Solmaz, M. B., and S. Uslu. 2023. Effects of turbuence and flamelet combustion modelling on the CFD simulation of a dual inlet ramjet combustor. *International Journal of Turbo & Jet Engines*. <https://doi.org/10.1515/tjj-2023-0039>
- Solmaz, M. B., S. Uslu, and O. Uzol. 2014. Unsteady RANS for Simulation of High Swirling Non-Premixed Methane-Air Flame. *50th AIAA/ASME/SAE/ASEE Joint Propulsion Conference*. AIAA Paper 2014-3473. <https://doi.org/10.2514/6.2014-3473>
- Spalart, P. R., S. Deck, M.L. Shur, K.D. Squires, M.K. Strelets, and A. Travin. 2006. A New Version of Detached-Eddy Simulation, Resistant to Ambiguous Grid Densities. *Theoretical and Computational Fluid Dynamics*. 20(3):181-195. <https://doi.org/10.1007/s00162-006-0015-0>
- Spalart, P. R., W-H. Jou, M.K. Strelets, and S. R. Allmaras. 1997. Comments on the feasibility of LES for wings, and on a hybrid RANS/LES approach. 1st AFOSR Int. Conf. on DNS/LES, Aug. 4-8, 1997, Ruston, LA. In *Advances in DNS/LES*, C. Liu & Z. Liu Eds., Greyden Press, Columbus, OH
- Stowe, R.A., C. Dubois, P.G. Harris, A.E.H.J. Mayer, A. deChamplain, and S. Ringuette. 2004. Performance Prediction of a Ducted Rocket Combustor Using a Simulated Solid Fuel. *Journal of Propulsion and Power*. 20(5):936-944. <https://doi.org/10.2514/1.2799>
- Stull, F.D., R.R. Craig, G.D. Streby, and S. P. Vanka. 1985. Investigation of a Dual Inlet Side Dump Combustor Using Liquid Fuel Injection. *Journal of Propulsion and Power*. 1(1):83-88. <https://doi.org/10.2514/3.22763>
- Sun, M.-B., Z.-G. Wang, J.-H. Liang, and H. Geng. 2008. Flame Characteristics in Supersonic Combustor with Hydrogen Injection Upstream of Cavity Flameholder. *Journal of Propulsion and Power*. 24(4):688-95. <https://doi.org/10.2514/1.34970>
- Timnat, Y.M. 1990. Recent Developments In Ramjets, Ducted Rockets And Scramjets. *Progress in Aerospace Sciences*. 27(3):201-235. [https://doi.org/10.1016/0376-0421\(90\)90007-7](https://doi.org/10.1016/0376-0421(90)90007-7)
- Travin, A., M. Shur, M. Strelets, and P.R. Spalart. 2002. Physical and Numerical Upgrades in the Detached-Eddy Simulation of Complex Turbulent Flows. In *Advances in LES of Complex Flows*. ed. R. Friedrich, W. Rodi. Springer Netherlands, Dordrecht. https://doi.org/10.1007/0-306-48383-1_16
- Williams, F.A. 1975. Recent Advances in Theoretical Descriptions of Turbulent Diffusion Flames. In *Turbulent Mixing in Nonreactive and Reactive Flows*, ed. S.N.B. Murthy. Springer New York. https://doi.org/10.1007/978-1-4615-8738-5_5
- Yang, S., X. Wang, W. Sun, and V. Yang. 2020. Comparison of Finite Rate Chemistry and Flamelet/Progress-Variable Models: Sandia Flames and the Effect of Differential Diffusion. *Combustion Science and Technology*. 192(7):1137-1159. <https://doi.org/10.1080/00102202.2020.1754809>